INTERNATIONAL JOURNAL FOR NUMERICAL METHODS IN FLUIDS, VOL. 4, 459–475 (1984)

FINITE ELEMENT SIMULATION OF DIP COATING, II: NON-NEWTONIAN FLUIDS*

P. TANGUY†§, M. FORTIN‡ AND L. CHOPLIN†

Université Laval, Cité Universitaire, Québec, QC, Canada, G1K 7P4

SUMMARY

We apply in this paper the augmented Lagrangian method to the study of various non-Newtonian fluid flow problems, and in particular the dip coating process. We only present in this second part the treatment specific to the non-linearities involved in the constitutive equations, the first part having largely been concerned with the general description of the approximation used.

Two rheological models illustrating different rheological behaviours are used to simulate dip coating process: the Carreau-A model for shear-thinning properties of the viscosity and a truncated second-order model for a Newtonian behaviour in viscosity with elastic properties.

Numerical predictions show a very good agreement with experimental data for the second-order model. The discrepancy observed in the other case can be explained qualitatively by the elastic properties exhibited by the shear-thinning fluids used: this elasticity is not taken into account in the Carreau-A model.

KEY WORDS Augmented Lagrangian Finite Element Method Dip Coating Non-Newtonian Fluids

1. INTRODUCTION

In the first part of this work,[1] we have shown that the finite element method coupled to a pseudo-time stepping technique is suitable to predict the meniscus shape, one of the main characteristics of the dip coating process, in the case of Newtonian fluids. Most coating fluids, however, are polymeric fluids and Newton's law of viscosity is completely inadequate for describing the relation between the stress components and the velocity gradients, called the constitutive equation or rheological equation of state. General constitutive equations lead to non-linear problems. We shall develop, in this second part, a quite general procedure to deal with these non-linearities. We shall then consider two types of constitutive equations, each one representing two of the most important characteristics of the polymeric fluids used in coating processes: shear-thinning and elasticity.

The first constitutive equation is a simple extension of the Newtonian model and is called generalized Newtonian fluid (GNF) model. It can describe the shear rate dependence of the viscosity and several empiricisms are available for this. Because shear-thinning (monotonic decrease of viscosity with increasing shear rate) is the most commonly encountered shear rate dependence of viscosity for polymeric fluids, we have chosen the model A of Carreau,

---

* Presented in part at the 5th Canadian Symposium on Fluid Dynamics, Windsor (Ontario), Canada, 6–9 June, 1982.

† Department of Chemical Engineering

‡ Department of Mathematics

§ Present address: Dept. of Chem. Eng., TUNS, POB 1000, Halifax, NS, Canada, B3J 2X4

0271–2091/84/050459–17$01.70

Received September 1982
Revised February 1983

which has been proved to fit fairly well the shear-thinning behavior for a great variety of these fluids, contrarily to the classical and widely used power-law model.[2]

The second equation can be seen as an extension of the previous GNF model, as well as a truncation of a more general expression for the stress tensor for a very wide class of fluids, the Criminale–Ericksen–Filbey (CEF) equation, which is itself a simplification of the Reiner–Rivlin equation.[2] If we define the rate-of-strain tensor by:

$$\dot{\boldsymbol{\gamma}} = \tfrac{1}{2}[\boldsymbol{\nabla}\mathbf{v} + (\boldsymbol{\nabla}\mathbf{v})^{\mathrm{T}}] \tag{1}$$

the constitutive equation we will use is written as follows:

$$\boldsymbol{\tau} = -2\eta_0\dot{\boldsymbol{\gamma}} - 2\Psi_1\{\dot{\boldsymbol{\gamma}}\cdot\dot{\boldsymbol{\gamma}}\} \tag{2}$$

where η_0 is a parameter associated with the viscosity of the fluid and Ψ_1 is the first normal stress coefficient related to its elasticity. They are defined customarily in shear flows. Choosing these parameters to be constant means that the viscosity will remain constant (Newtonian behaviour) and that the first normal stress difference, N_1, related to Ψ_1 by the relation:

$$\Psi_1 = \frac{N_1}{4\dot{\gamma}_{yx}^2} = -\frac{\tau_{xx} - \tau_{yy}}{4\dot{\gamma}_{yx}^2} \tag{2'}$$

shows a quadratic dependence on rate-of-strain, which is typical of a so-called second-order fluid.[2] In equation (2′) x is the direction of flow and y is the direction of the velocity gradient.

For polymeric fluids, it is extremely rare to find shear-thinning without elasticity and vice versa. It seems then *a priori* unreasonable to work with such simplified constitutive equations, one describing a shear-thinning behaviour alone, the other an elastic behaviour without any shear-thinning. The reasons given by Bird *et al.*[2] for justifying the use of GNF models as well as second-order models instead of more realistic rheological equations of state in such situations of flow slightly outside of the region of legitimacy of these models can appear to be sufficient. We have to add, however, the purely mathematical interest of the use of such models. Another justification can be found for the use of the second-order model defined by equation (2): recently, some remarkably interesting rheological properties have been found for a fluid[3] allowing not only valuable comparison between numerical predictions and experimental data but also to determine or identify the role of normal stresses (i.e. 'elasticity') in a determinate situation of flow.

The addition of such constitutive relations to the equations of change governing the dynamics of flow problems introduces new non-linearities whose treatment requires peculiar attention. Only a few particular non-Newtonian problems have been solved.[4] The purpose of this second part is to present an extension to the study of non-Newtonian flow problems and in particular to the dip coating problem of a method developed by Fortin and Glowinski,[5] called the augmented Lagrangian method, which has been used in electromagnetism[6] and has been proved to be applicable, particularily when a non-linearity is related to the unknown gradients, i.e. the velocity gradients.

2. THE AUGMENTED LAGRANGIAN METHOD

2.1. Basic principles

Let us consider the equations governing the steady isothermal flow of a generalized

Newtonian fluid. We have, as in part I:

$$\nabla.\tau^{D}+\nabla p+(\mathbf{v}.\nabla)\mathbf{v}=\mathbf{f} \tag{3}$$

$$\nabla.\mathbf{v}=0 \tag{4}$$

$$\tau^{D}=-2\eta(|\dot{\gamma}|)\dot{\gamma}(\mathbf{v})=\phi(|\dot{\gamma}|^{2})\dot{\gamma}(\mathbf{v}) \tag{5}$$

We denote by τ^{D} the deviatoric of the viscous stress tensor, $\mathbf{v}$ is the velocity, p the pressure and $\mathbf{f}$ a body force. We denote by $\dot{\gamma}$ the rate of strain tensor and by $|\dot{\gamma}|$, its second invariant ($|\dot{\gamma}|=\sqrt{(\dot{\gamma}:\dot{\gamma})}$).

Equation (5) is the constitutive relation of the fluid. It relates the viscosity η and the rate-of-strain tensor to the stress tensor. For a Newtonian fluid, η is constant. For a generalized Newtonian fluid, we have a relation between η and $|\dot{\gamma}|$.

We refer to part I for a description of the boundary conditions needed to specify the dip coating flow problem. In order to associate with Problem (3)–(5) a variational principle in the classical sense (minimization of a functional) we temporarily neglect inertial terms in (3).

Defining $\Phi(y)$ by:

$$\frac{\partial}{\partial y}\Phi(y)=\phi(y), \qquad \Phi(0)=0 \tag{6}$$

solving (3)–(5) is equivalent to the minimization of

$$J(\mathbf{v})=\int_{\Omega}\Phi(|\dot{\gamma}|^{2})\,dx-\int_{\Omega}\mathbf{f}.\mathbf{v}\,dx \tag{7}$$

under the constraint $\nabla.\mathbf{v}=0$.

A direct use of (7) in a finite element method leads to a set of non-linear equations. This implies that one must solve this problem using an iterative technique, in general by solving a sequence of linear problems. Solving a large linear system can be done in two steps: factoring the matrix and solving the computed factors. The first operation is much more time consuming than the second, so that solving a sequence of linear problems with a fixed matrix is much less expensive than an analogue sequence in which the matrix has to be factored at each step. The augmented Lagrangian method reaches this goal by a decomposition method that restricts the non-linearity to 'local' point-wise problems. To do so, we introduce, following Reference 5, an auxiliary tensor $\boldsymbol{\sigma}$ and we minimize (with $\nabla.\mathbf{v}=0$):

$$\tilde{J}(\mathbf{v},\boldsymbol{\sigma})=\int_{\Omega}\Phi(|\boldsymbol{\sigma}|^{2})\,dx-\int_{\Omega}\mathbf{f}.\mathbf{v}\,dx \tag{8}$$

under the constraint $\boldsymbol{\sigma}=\dot{\gamma}(\mathbf{v})$. This is of course a mere trivial restatement of the problem. We now deal with the constraint by the simultaneous use of a Lagrange multiplier and a penalty term in the spirit of the multiplier method of Hestenes[7] and Powell.[8] We thus define the augmented Lagrangian (that also takes into account the constraint $\nabla.\mathbf{v}=0$):

$$\mathscr{L}_{r}(\mathbf{v},p,\boldsymbol{\sigma},\boldsymbol{\lambda})=\int_{\Omega}\Phi(|\boldsymbol{\sigma}|^{2})\,dx-\int_{\Omega}p\nabla.\mathbf{v}\,dx-\int_{\Omega}\mathbf{f}.\mathbf{v}\,dx$$
$$+\int_{\Omega}a(x)[\boldsymbol{\lambda}:(\boldsymbol{\sigma}-\dot{\gamma}(\mathbf{v})]\,dx+\frac{r}{2}\int_{\Omega}a(x)\,|\boldsymbol{\sigma}-\dot{\gamma}(\mathbf{v})|^{2}\,dx \tag{9}$$

The factor $a(x)$ is used to rescale the $L^{2}(\Omega)$ scalar product and we shall discuss later its role

as a convergence accelerator. It can be taken equal to one, but the optimal choice is to use the best available estimate of $\eta(|\dot{\gamma}|)$. r is a penalty parameter.

Let us consider the three equilibrium equations describing a saddle-point of the Lagrangian $\mathscr{L}_r$. The variational equations, obtained by solving in $\mathbf{v}$, p when $\boldsymbol{\sigma}$ and $\boldsymbol{\lambda}$ are fixed, can be written:

$$\left.\begin{aligned} r\int_\Omega a(x)\dot{\boldsymbol{\gamma}}(\mathbf{v}):\dot{\boldsymbol{\gamma}}(\delta\mathbf{v})\,dx - \int_\Omega a(x)(\boldsymbol{\lambda}+r\boldsymbol{\sigma}):\dot{\boldsymbol{\gamma}}(\delta\mathbf{v})\,dx \\ -\int_\Omega p\boldsymbol{\nabla}.\delta\mathbf{v}\,dx - \int_\Omega \mathbf{f}.\delta\mathbf{v}\,dx = 0 \\ \int_\Omega \delta p\boldsymbol{\nabla}.\mathbf{v}\,dx = 0, \quad \forall\delta\mathbf{v}, \quad \forall\delta p \end{aligned}\right\} \tag{10}$$

where $\delta\mathbf{v}$ and δp (the variations of $\mathbf{v}$ and p) are to be chosen in an appropriate functional space taking into account essential boundary conditions. Problem (10) is a linear problem of Stokes type with a variable viscosity coefficient $a(x)$.

Solving in $\boldsymbol{\sigma}$, $\mathbf{v}$, p and $\boldsymbol{\lambda}$ being given, yields the equation:

$$\int_\Omega [\eta(|\boldsymbol{\sigma}|)+ra(x)]\boldsymbol{\sigma}:\delta\boldsymbol{\sigma}\,dx - \int_\Omega a(x)[r\dot{\boldsymbol{\gamma}}(\mathbf{v})-\boldsymbol{\lambda}]:\delta\boldsymbol{\sigma}\,dx = 0 \tag{11}$$

This equation contains no derivative and can be shown to be equivalent to an (infinite) set of point-wise equations:

$$[\eta(|\boldsymbol{\sigma}|)+ra(x)]\boldsymbol{\sigma}(x) - a(x)[r\dot{\boldsymbol{\gamma}}(\mathbf{v}(x))-\boldsymbol{\lambda}(x)] = 0, \qquad \forall x\in\Omega \tag{12}$$

Finally the optimality condition in λ is nothing but the constraint

$$\boldsymbol{\sigma} = \dot{\boldsymbol{\gamma}}(\mathbf{v}) \tag{13}$$

We shall now proceed to the discretization of these equations and then consider an iterative method using the discrete analogues of (10), (12) and (13) to compute the solution of the problem. Before doing so, we shall consider two examples of constitutive relations, in order to illustrate the decomposition principle.

Example 1: *Carreau-A model.* We consider, following Carreau,[9] the constitutive equation:

$$\boldsymbol{\tau}^D = -\eta_0[1+|t_c\dot{\boldsymbol{\gamma}}(\mathbf{v})|^2]^{-S}\dot{\boldsymbol{\gamma}}(\mathbf{v}) \tag{14}$$

The function $\Phi(\sigma)$ is easily seen to be:

$$\Phi(\sigma) = \frac{\eta_0}{2(1-S)t_c^2}[(1+t_c^2|\boldsymbol{\sigma}|^2)^{1-S}-1] \tag{15}$$

and equation (12) becomes point-wise:

$$\left(\frac{\eta_0}{[1+t_c^2|\boldsymbol{\sigma}|^2]^S}+ra(x)\right)\boldsymbol{\sigma} = a(x)[r\dot{\boldsymbol{\gamma}}(\mathbf{v})-\boldsymbol{\lambda}] \tag{16}$$

This tensor equation can be reduced to a scalar equation. Indeed $|\boldsymbol{\sigma}|$ satisfies the equation:

$$\left[\frac{\eta_0}{(1+t_c^2|\boldsymbol{\sigma}|^2)^S}+r(x)\right]|\boldsymbol{\sigma}| = a(x)\,|r\dot{\boldsymbol{\gamma}}(\mathbf{v})-\boldsymbol{\lambda}| \tag{17}$$

Such a non-linear one-dimensional problem can be solved very simply by a classical method, such as Newton's method. When $|\boldsymbol{\sigma}|$ is known, this value can be inserted in (16) which then becomes a set of uncoupled linear equations. The use of the augmented Lagrangian in this case fully satisfies the condition of Reference 5 and can be completely justified.

Example 2: *second-order model.* This example is a formal extension of the above development. It shows that the method can be applied to cases where it cannot be rigorously proved to work. We consider the constitutive equation equivalent to (2):

$$\boldsymbol{\tau}^{D} = -2\eta_0\dot{\boldsymbol{\gamma}} - 2\Psi_1(\dot{\boldsymbol{\gamma}}.\dot{\boldsymbol{\gamma}}) = (-2\eta_0\boldsymbol{\delta} - 2\Psi_1\dot{\boldsymbol{\gamma}}).\dot{\boldsymbol{\gamma}} \tag{18}$$

where $\boldsymbol{\delta}$ is the unit tensor, or:

$$\boldsymbol{\tau}^{D} = -\boldsymbol{\eta}(\dot{\boldsymbol{\gamma}}).\dot{\boldsymbol{\gamma}} \tag{18'}$$

This can thus be seen as a generalized Newtonian fluid in which viscosity is no longer isotropic and is defined by a tensor dependent on $\dot{\boldsymbol{\gamma}}(\mathbf{v})$. It is no longer possible to find a function Φ and to write the Lagrangian $\mathscr{L}_r$. It is however possible to consider equations (10), (12) and (13). In particular (12) becomes:

$$2\eta_0\boldsymbol{\sigma} + 2\Psi_1\boldsymbol{\sigma}.\boldsymbol{\sigma} + ra(x)\boldsymbol{\sigma} = a(x)(r\dot{\boldsymbol{\gamma}}(\mathbf{v}) - \boldsymbol{\lambda}) \tag{19}$$

This is a set of 4 or 5 (depending if a plane or an axisymmetric problem is considered) non-linear equations. Newton's method can be used provided a reasonable initial estimate is available.

2.2. *Discretization*

With respect to the approximation of a Newtonian flow, the procedure we follow requires no real change. The approximation of $\mathbf{v}$ and p was done using the Q_{93} and T_{73} elements as in Part I. The approximation of problem (10) is then a straightforward procedure and was done exactly as in the Newtonian case. The only really tricky thing is the discretization of variables $\boldsymbol{\lambda}$ and $\boldsymbol{\sigma}$. The components of $\boldsymbol{\sigma}$ should at the limit be equal to the components of $\dot{\boldsymbol{\gamma}}(\mathbf{v})$. If $\mathbf{v}$ is approximated by a biquadratic polynomial, the components of $\dot{\boldsymbol{\gamma}}(\mathbf{v})$ are themselves in a subspace of biquadratic polynomials. We chose to approximate, on each element, $\boldsymbol{\sigma}$ by a biquadratic on quadrilateral elements and by a quadratic on triangular elements.

There is *no continuity requirement* on these functions. Moreover, the degrees of freedom of these functions were defined using as nodal values either the points of a 3×3 Gaussian formula on the reference element for quadrilaterals or the 6 points of a Gaussian formula on the reference element for quadrilaterals or the 6 points of a Gaussian formula accurate for polynomials of degree 4 on triangles.[10] These quadrature formulae are then *exact* to compute integrals, such as $\int_\Omega \boldsymbol{\sigma}:\boldsymbol{\lambda}\,dx$ appearing in the augmented Lagrangian. The shape functions associated with these nodes are then orthogonal with respect to the quadrature formulae or even for the exact integration. Finally the term $\int_\Omega \Phi(|\boldsymbol{\sigma}|)\,dx$ is evaluated using the same quadrature formulae.

This yields a discrete equivalent of Equation (11) that can be uncoupled on each numerical integration point. If other nodal values had been chosen for $\boldsymbol{\sigma}$, we would have to solve a set of non-linear equations on each element. The values of $\boldsymbol{\lambda}$ are also defined at the same points

so that using the same quadrature rule to evaluate in Equation (10)

$$\int_\Omega a(x)[\boldsymbol{\lambda}+r\boldsymbol{\sigma}]:\dot{\boldsymbol{\gamma}}(\delta\mathbf{v})\,dx$$

$a(x)$ being constant per element.

We only need to know the nodal values of $\boldsymbol{\lambda}$ and $\boldsymbol{\sigma}$, and the shape functions are in fact *never explicitely used.*

2.3. *The iterative algorithm*

The maximization in $\boldsymbol{\lambda}$ is obtained by an iterative process, called ALG2 in Reference 5. When the stability of the numerical solutions is reached, both $\boldsymbol{\lambda}$ and $\boldsymbol{\sigma}$ are equal to $\dot{\boldsymbol{\gamma}}(\mathbf{v})$. It is then possible to test the stability either by imposing a criterion on two successive values of $\boldsymbol{\lambda}$ or classically by testing the velocity values. It has been shown[5] that, for some classes of problems, the convergence in $\boldsymbol{\lambda}$ and $\mathbf{v}$ can be uncoupled, that is $\boldsymbol{\lambda}$ has not converged although $\mathbf{v}$ has done. In our problem, we have noticed it was not the case then the classical alternative has been used to stop the computation. The algorithm is then organized as follows:

(i) $\boldsymbol{\lambda}^0$, p^0, $\mathbf{v}^0$ being given arbitrarily or from available data, factorize the stiffness matrix.

At the ith iteration:

(ii) compute $\boldsymbol{\sigma}^i$ from $\boldsymbol{\lambda}^{i-1}$, $\mathbf{v}^{i-1}$ by minimizing $\mathscr{L}_{\mathrm{rh}}(\boldsymbol{\sigma}^i, \mathbf{v}^{i-1}, \boldsymbol{\lambda}^{i-1})$ in $\boldsymbol{\sigma}$ (Equation (12)),

(iii) update $\boldsymbol{\lambda}$ by $\boldsymbol{\lambda}^i = \boldsymbol{\lambda}^{i-1} + r(\boldsymbol{\sigma}^i - \dot{\boldsymbol{\gamma}}^{i-1}(\mathbf{v}^{i-1}))$

(iv) solve a Stokes problem in $\mathbf{v}^i$ that is minimize $\mathscr{L}_{\mathrm{rh}}(\boldsymbol{\sigma}^i, \mathbf{v}, \boldsymbol{\lambda}^i)$ in $\mathbf{v}$ (equation (10))

(v) test the convergence by $\max\left|\dfrac{\mathbf{v}^i - \mathbf{v}^{i-1}}{\mathbf{v}^{i-1}}\right| < 10^{-2}$ and return to step (ii) if necessary.

This method is shown to converge by Fortin and Glowinski[5] for a wide class of problems containing in particular the Carreau-A model. A crucial point to get good convergence properties is to make a good choice of $a(x)$. It is also shown that $a(x)$ should be an estimate of the actual viscosity $\eta(\dot{\boldsymbol{\gamma}}(\mathbf{v}))$. It is possible to compute a good value of $a(x)$ using some initial estimate of $\mathbf{v}$. This is usually done in some incremental procedure proceeding to 'more and more non-linear' problems and using the previous solution to estimate $a(x)$. This is what was done in our computations on Carreau-A model moving from $S = 0$ (Stokes flow) to $S = 0{\cdot}4$, corresponding to a highly non-linear problem. For a properly chosen $a(x)$ it can be shown[5] that the best choice for the penalty parameter is $r = 1$. Indeed, with such a choice, the linear problem can be proved to converge in one iteration.

3. NUMERICAL TESTS

In order to evaluate the performance of the algorithm, we have simulated a simple shear flow in a circular tube of an inelastic fluid whose rheological behaviour follows the Carreau-A model of viscosity. The fluid selected is a solution of Polystyrene in a solvent called Aroclor, for which rheological data were available.[11] This simulation has been performed with two sets of boundary conditions.

(i) The first configuration (shown in Figure 1) consists of imposing a pressure loss between the inlet and the outlet of the tube. For such a situation, a pseudo-analytical solution can be derived which allows evaluation of the accuracy of computational results. Indeed, for a given pressure loss in a circular tube, the momentum equations can be

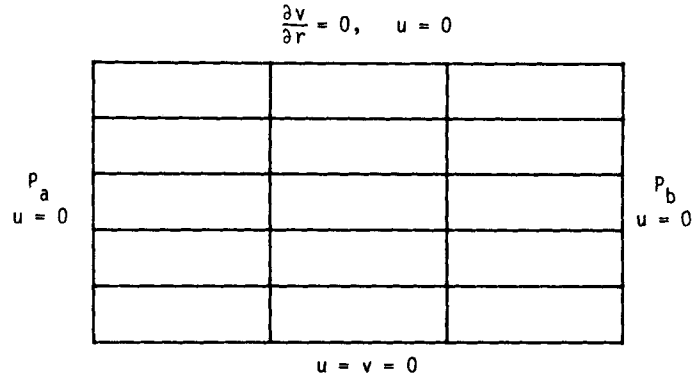

Figure 1. Imposed pressure loss in a circular tube: grid and boundary conditions

written in steady-state as follows:

$$\eta_0[1+(t_c\dot{\gamma})^2]^{-s}\frac{dv_z}{dr} = -\frac{\Delta P}{2L}r \tag{20}$$

where $\dot{\gamma}$, the magnitude of the rate of strain tensor $\dot{\boldsymbol{\gamma}}$, which is a rate of shear tensor in this case, reduced to $\left(-\frac{1}{\sqrt{2}}\frac{dv_z}{dr}\right)$. ΔP is the pressure loss, L the length of the tube and r the radial coordinate. v_z is the component of $\mathbf{v}$ in the direction of flow. This equation is non-linear, then the solution is obtained iteratively by the Newton's method. Once dv_z/dr has been calculated for various values of r, the velocity profile is obtained by integrating the shear rate with respect to r by the Simpson's rule. Two tests have been performed: one deals with the error of discretization, that is determines the influence of the mesh size; the other with the error due to the calculation of the non-linearity node by node. Indeed, since the non-linear term is not polynomial, its evaluation by a quadrature formula leads to introduce errors in the computation.

(ii) the second configuration (shown in Figure 2) was used to test the behaviour of the algorithm when the physical problem becomes highly non-linear, that is in the case of strong shear-thinning. In order to do this, a flow rate is imposed as inlet condition (under the form of a Poiseuille flow) whereas at the outlet, we assume that the flow is

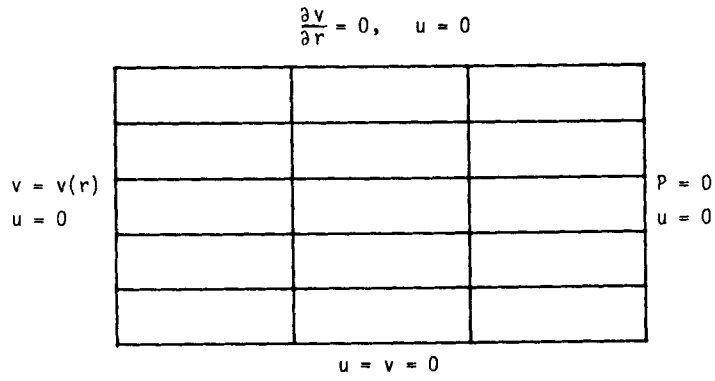

Figure 2. Imposed flow rate in a circular tube: grid and boundary conditions

fully developed. With such conditions, a choice of initial guess like a Poiseuille flow allows fast convergence.

The physical problem being axisymmetrical, the solution is sought between the centre line of the tube and the wall, whatever the configuration.

The only non-linear effect in these tests is caused by the rheological behaviour of the fluid considered. In Figure 3 we show the typical evolution of the viscosity with the shear rate according to the Carreau-A model. When $S = 0$, the behaviour is Newtonian, and increasing S corresponds to increasing shear-thinning. We have superimposed in Figure 4, for four values of S, the numerical solution (represented by symbols) and the pseudo-analytical solution (represented by a full line). These results have been obtained with the finite element grid and the boundary conditions presented in Figure 1. The comparison of the computational results with the pseudo-analytical solution exhibits a noteworthy agreement. The observations of the four curves in Figure 4 shows that the flow rate increases with increasing S.

Moreover a very slight amount of shear-thinning is sufficient to increase the flow rate significantly. Convergence is reached after few iterations if the problem is weakly non-linear;

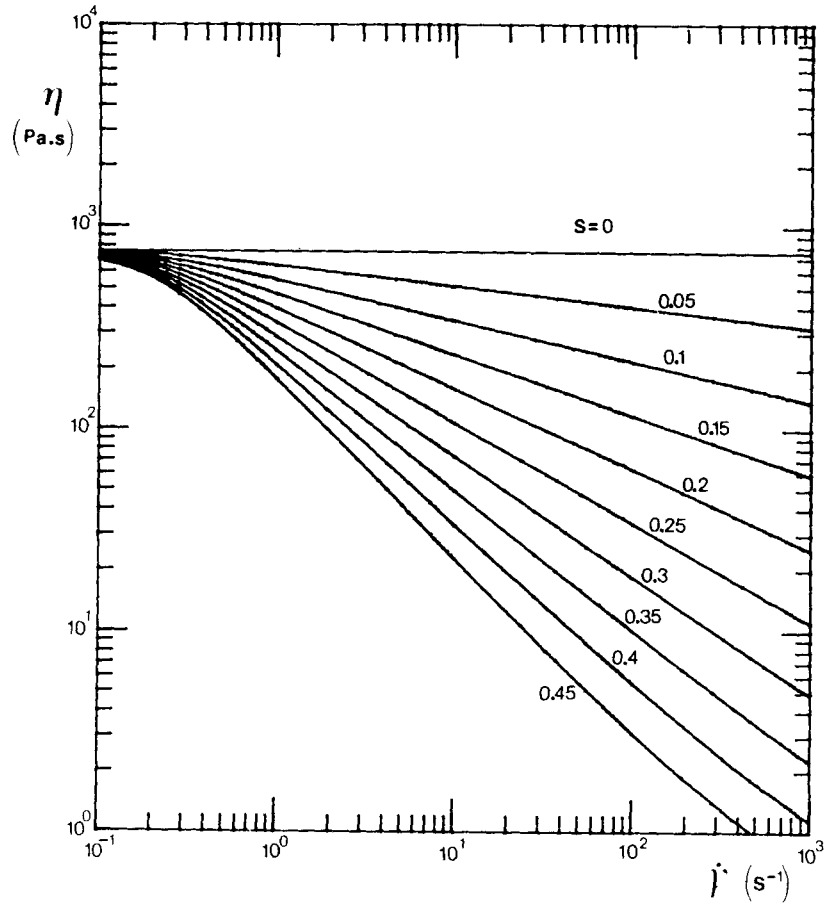

Figure 3. Viscosity as function of shear rate as predicted by the Carreau model (η_0, t_c and η_∞ are constant) for parameter S varying from 0 to 0·45

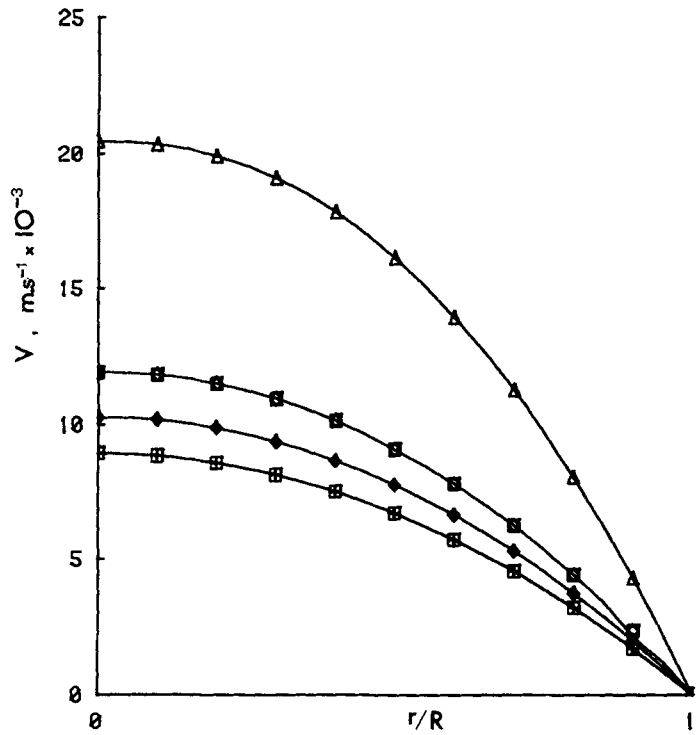

Figure 4. Developed velocity profile for given value of ΔP: —, analytical or pseudo-analytical solution; numerical results: ⊞, $S = 0$; ⊕, $S = 0{\cdot}02$; ⊠, $S = 0{\cdot}04$; △, $S = 0{\cdot}1$

the number of iterations increases rapidly when S is augmented. According to the initial guess of velocity, it is necessary to compute ten to twenty iterations to get stable numerical predictions. The technique adopted to reduce computing time is to use as initial guess of $\mathbf{v}$ and $\boldsymbol{\lambda}$ for a given problem the results of the previous problem where the value of S is lower. If such data are not available, an incremental loading of S is performed.

In Figure 3, we also present the curves of viscosity versus shear rate for extreme values of S. It is important to point out that, according to our knowledge, no fluid exhibits shear-thinning more pronounced than that corresponding to values of S higher than 0·4. These curves are drawn from $S = 0$ to $S = 0{\cdot}45$ for the same values of the other parameters of the Carreau-A model. Computational tests have been performed for each value of S shown in Figure 3, and results are presented in Figures 5–7. In all cases, we used the second set of boundary conditions shown in Figure 2, that is we imposed the flow rate. We see a rearrangement of the velocity profile from a parabolic form ($S = 0$) to a flat profile (quasi plug flow) for $S = 0{\cdot}45$. Even for this extreme case of non-linearity, numerical convergence is obtained without difficulty.

The results of the error study are presented in Figure 8 as well as in Table I. For a medium ranged value of S ($S = 0{\cdot}1$) and for a given pressure loss, we have attempted to evaluate the error of discretization by varying the number of radial elements. The results show that the larger the number of elements, the smaller the error, which is logical. Accuracy of the method and of the elements is however noteworthy, since the error of discretization is in h^4.

Table I shows the error of computation which occurs when one increases the value of S. For slight shear-thinning, this error is negligible. For highly non-linear behaviour, the error

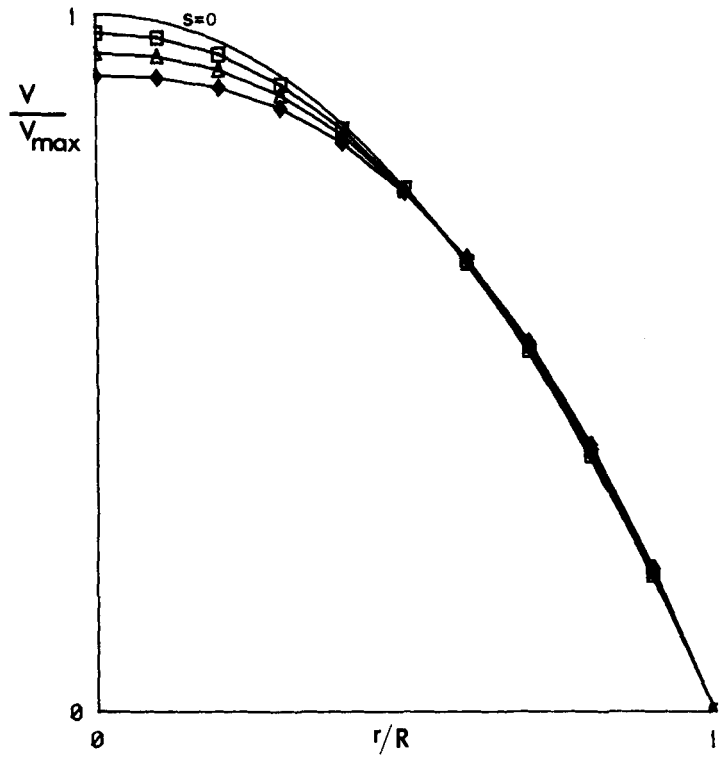

Figure 5. Developed velocity profile for given value of volumetric flow rate: —, analytical or pseudo-analytical solution; numerical results: □, $S = 0{\cdot}05$; △, $S = 0{\cdot}1$; ◆, $S = 0{\cdot}15$

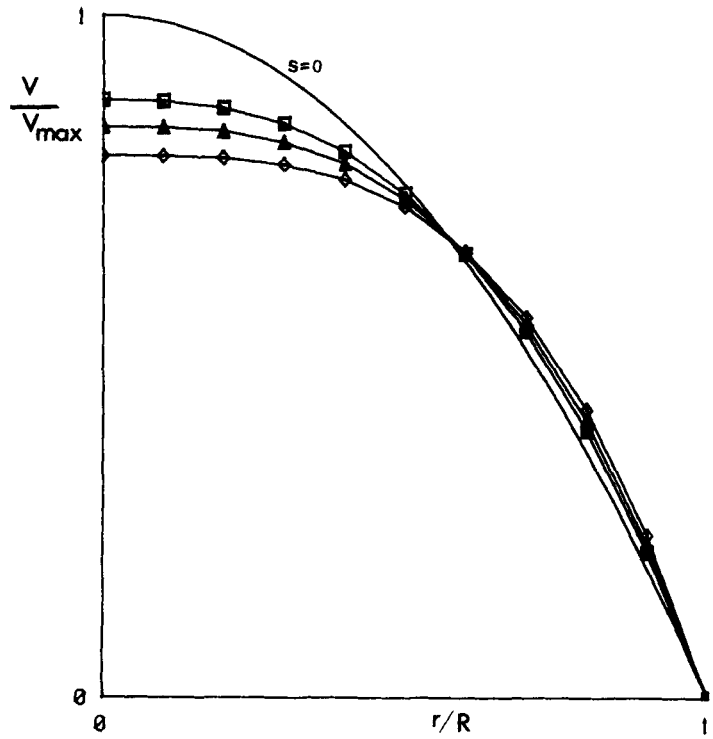

Figure 6. Developed velocity profile for given value of volumetric flow rate: —, analytical or pseudo-analytical solution; numerical results: ◪, $S = 0{\cdot}2$; ▲, $S = 0{\cdot}25$; ⊖, $S = 0{\cdot}3$

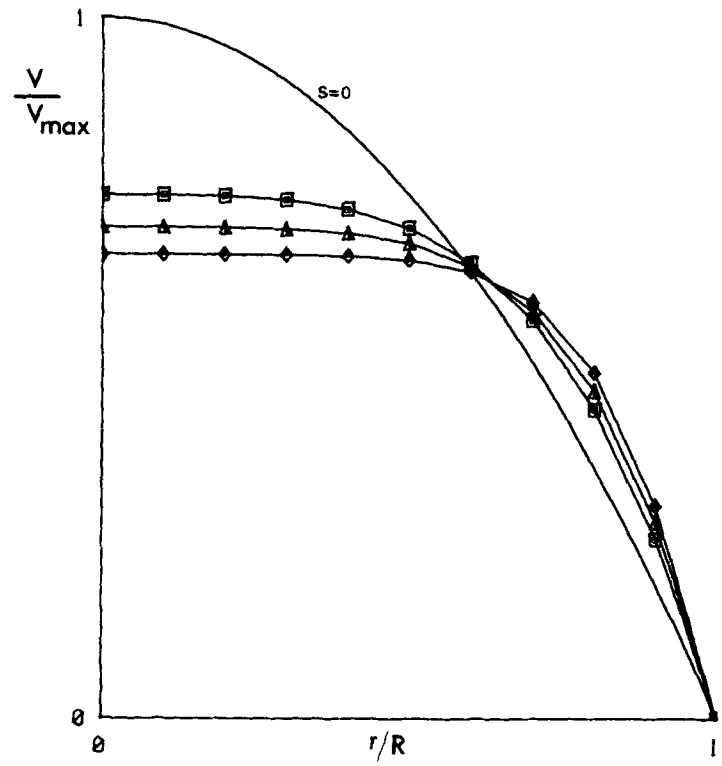

Figure 7. Developed velocity profile for given value of volumetric flow rate: —, analytical or pseudo-analytical solution; numerical results: ⊡, $S = 0{\cdot}35$; ▲, $S = 0{\cdot}4$; ◆, $S = 0{\cdot}45$

reached is far beyond the error of measurement which could be performed even with sophisticated apparatus. Thus, the method is seen to be very performant for a wide range of conditions.

Numerical tests for second-order fluid have also been performed. We have taken the data of Choplin *et al.*[3] for the parameters of equation (2). These data will be those corresponding to the fluid (Emkarox FC 31-45000) which we will use in dip coating. The conditions of the test were those given in Figure 2. For such a flow, an analytical solution of the equations of change can be easily derived which shows that the velocity profile is the same as in the Newtonian case. The numerical test has confirmed this equivalence.

4. THE DIP COATING PROBLEM

4.1. Boundary conditions and free surface algorithm

The augmented Lagrangian method is now applied to the study of wire dip coating with both previously mentioned non-Newtonian models. We refer to the first part of this work[1] for the boundary conditions (see Figure 9) and the statement of the problem, because they are the same as in Newtonian case. We also use the same algorithm for displacing the free surface, that is: we impose the natural boundary conditions for the Stokes problem solution and iteratively move the free surface with the aid of a pseudo-time stepping technique. The

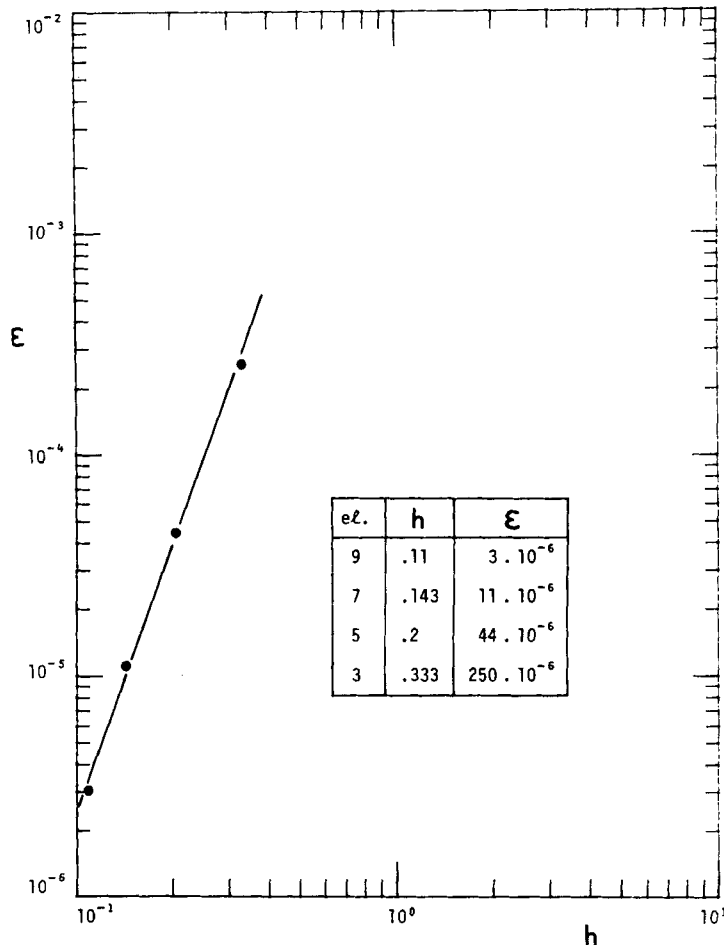

Figure 8. Error of discretization

Table I. Flow in a circular tube: comparison between pseudo-analytical and numerical velocity profiles for different values of the shear-thinning parameter.

	$S = 0{\cdot}02$			$S = 0{\cdot}2$			$S = 0{\cdot}25$		
r/R	$V_{P.A.}$ $\times 10^{-2}$	V_N $\times 10^{-2}$	$\Delta V/V_{P.A.}$ %	$V_{P.A.}$ $\times 10^{-2}$	V_N $\times 10^{-2}$	$\Delta V/V_{P.A.}$ %	$V_{P.A.}$ $\times 10^{-2}$	V_N $\times 10^{-2}$	$\Delta V/V_{P.A.}$ %
0	1·0249	1·0247	0·02	8·3012	8·3291	0·4	25·5466	25·6559	0·5
0·1	1·0155	1·0155	—	8·2814	8·3130	0·4	25·5170	25·6296	0·5
0·2	0·9865	0·9865	—	8·1844	8·1697	0·3	25·3315	25·4426	0·5
0·3	0·9371	0·9371	—	7·9618	7·9449	0·3	24·8352	24·9489	0·5
0·4	0·8670	0·8670	—	7·5742	7·5458	0·4	23·8751	23·9916	0·5
0·5	0·7759	0·7759	—	6·9868	6·9546	0·5	22·2998	22·4065	0·5
0·6	0·6636	0·6636	—	6·1675	6·1293	0·6	19·9592	20·0236	0·1
0·7	0·5300	0·5300	—	5·0867	5·0488	0·8	16·7051	16·7243	0·12
0·8	0·3750	0·3749	0.03	3·7161	3·6834	1	12·3906	12·3538	0·4
0·9	0·1983	0·1983	—	2·0291	2·0096	1	6·8702	6·8696	0·02
1·0	0	0	—	0	0	—	0	0	—

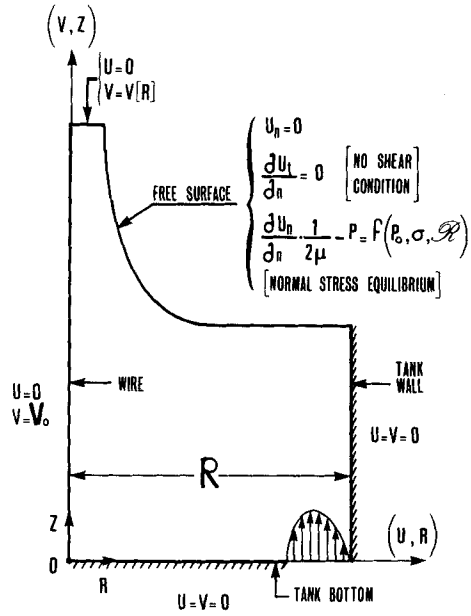

Figure 9. Boundary conditions for wire dip coating (at equilibrium)

displacement of this free surface is governed by the following equation:

$$\Delta x = \mathbf{x}^{k+1} - \mathbf{x}^{k} = \alpha(\mathbf{u}.\mathbf{n})\mathbf{n} \tag{21}$$

which is the same as equation (16) in Reference 1.

We remember here that α is a dummy time step, $\mathbf{u}.\mathbf{n} = u_n$ is the normal velocity at $\mathbf{x}^k$, which is a point of the free surface at step k, $\mathbf{n}$, the outward oriented normal and Δx, the displacement between steps k and $k+1$.

The natural boundary conditions are Neumann conditions and can be written on the free surface as follows:

$$\tau_{nt} = 0 \quad \text{(no shear condition)} \tag{22}$$

$$-p + \tau_{nn} = -p_0 - \frac{\sigma}{r\left[1+\left(\frac{dr}{dz}\right)^2\right]^{1/2}} + \frac{\sigma\frac{d^2r}{dz^2}}{\left[1+\left(\frac{dr}{dz}\right)^2\right]^{3/2}} \tag{23}$$

(normal stress equilibrium)

In the case of shear-thinning, the imposed velocity profile at the exit of the domain cannot be obtained analytically. It is calculated, for a given thickness h, by:

$$v(h) = \int_{r_0}^{h} \frac{dv_z}{dh}\,dh \tag{24}$$

where (dv_z/dh) is obtained by solving with a Newton's method the following unidirectional equation of change:

$$\eta(\dot{\gamma})\frac{\partial v_z}{\partial r} = \frac{\rho g}{2}\left(r - \frac{h^2}{2}\right) \tag{25}$$

Table II. Parameters of Carreau-A model

Fluid	η_0[=]Pa.s	t_c[=]s	S
Sodium alginate	211·46	9·7	0·21
Klucel M	16·76	3·3	0·18

provided we assume this expression is valid for describing the flow at the exit of the domain. The integration of $v(h)$ allows us to compute the flow rate and adjust with the imposed flow rate as described in Part I for the Newtonian case.

In the case of a second-order model, however, the imposed velocity profile, at the exit of the domain, will be exactly the same as in the Newtonian case, for a given value of the eventual coating thickness.

4.2. *Results and discussion*

The procedure which allowed us to obtain experimental data can be found elsewhere.[12] We will consider in this paper, only the direct comparison between these data and the numerical predictions.

In all cases presented, in order to save computing time, we have taken the experimental

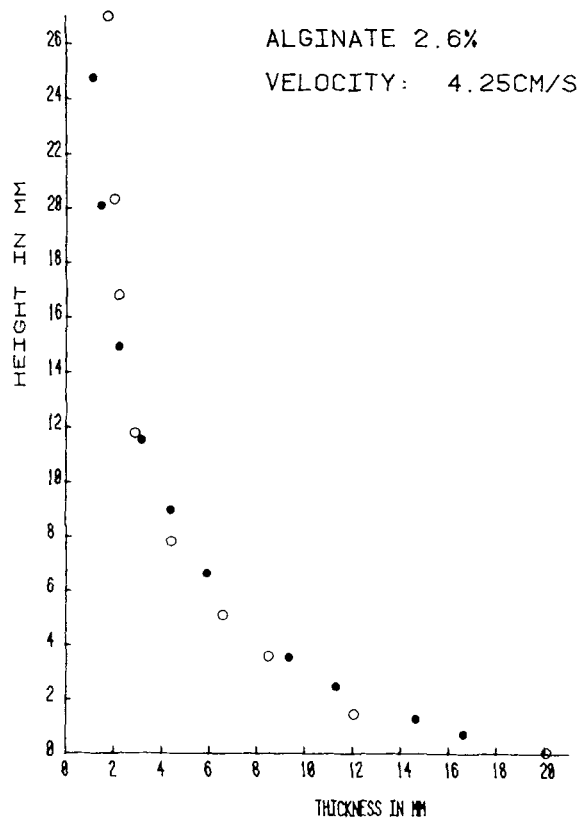

Figure 10. Meniscus profile for Sodium Alginate ($V_0 = 4.25$ cm/s): ○ numerical prediction; ● experimental measurement

data as the initial guess for the meniscus profile, but there is no doubt that any initial guess can be used.

4.2.1. *Carreau-A model.* We have worked with two polymeric liquids: a solution of 2·6 per cent in weight of sodium alginate in a glycerol–water mixture and a solution of 3 per cent in weight of Klucel M in a glycerol–water mixture. The rheological properties of these fluids have been obtained with a Rheometrics System Four. In both cases, the Carreau-A model fits fairly well the experimental values of the viscosity in a wide range of shear rate. The parameters of the model have been obtained through the use of a non-linear regression technique and are shown in Table II.

For both fluids, we measured first normal stress differences. We have mentioned previously that fluids exhibiting shear-thinning properties together with elastic properties are practically impossible to find. It is possible, however, to find shear-thinning fluids which are substantially less elastic than others; that is the reason of the choice of such fluids for which measured values of normal stress differences are relatively low. Therefore, in first approximation, the Carreau-A model can be considered sufficient to describe the rheological behaviour of these fluids.

The numerical predictions, however, as compared with experimental data, and shown in Figures 10 and 11, as well as in Table III for the eventual coating thickness disprove this

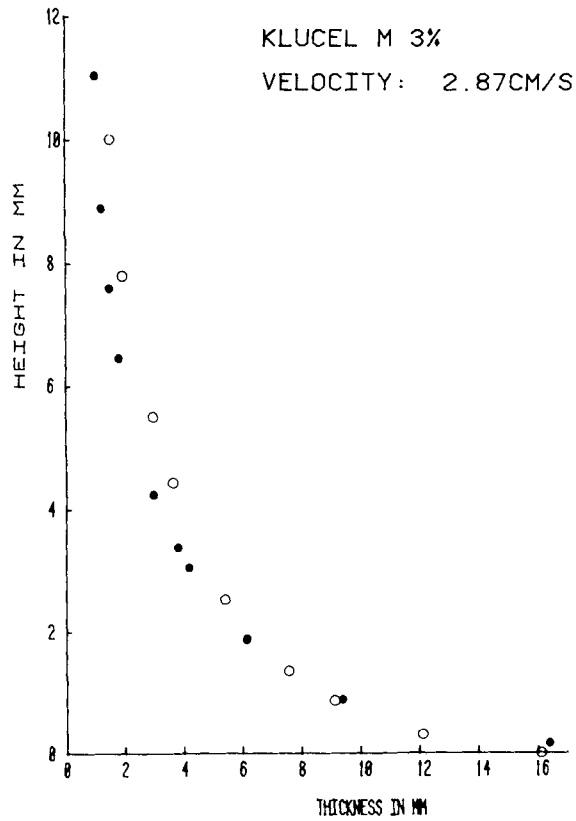

Figure 11. Meniscus profile for Klucel M ($V_0 = 2{\cdot}87$ cm/s): ○ numerical prediction; ● experimental measurement

Table III. Eventual coating thickness: comparison between experimental data and numerical predictions

Fluid	V_0 [=] m/s	h_{num} [=] mm	h_{exp} [=] mm
Sodium alginate	0·0425	1·91	1·02
Klucel M	0·0287	1·44	0·85
Emkarox FC 31-45000	0·0089	3·18	3·26

assumption. We observed a not negligible discrepancy in the whole meniscus, indicating that it will be necessary to take into account the normal stresses exhibited by the fluids.

Moreover, the dip coating flow situation presents a relatively important difference with respect to the shear flows we used in the numerical tests. Only the upper part of the meniscus is in steady shear flow. In the remaining part, we have a superimposition of steady shear and elongational flows. Despite the fact that we only considered creeping flow, the behaviour of fluids exhibiting both shear-thinning and elastic properties in such situations is far from completely understood and well known, and will certainly affect the shape of the meniscus. The main conclusion is that shear-thinning is not sufficient to describe the rheological behaviour of these apparently very weakly elastic fluids even at low shear-rates.

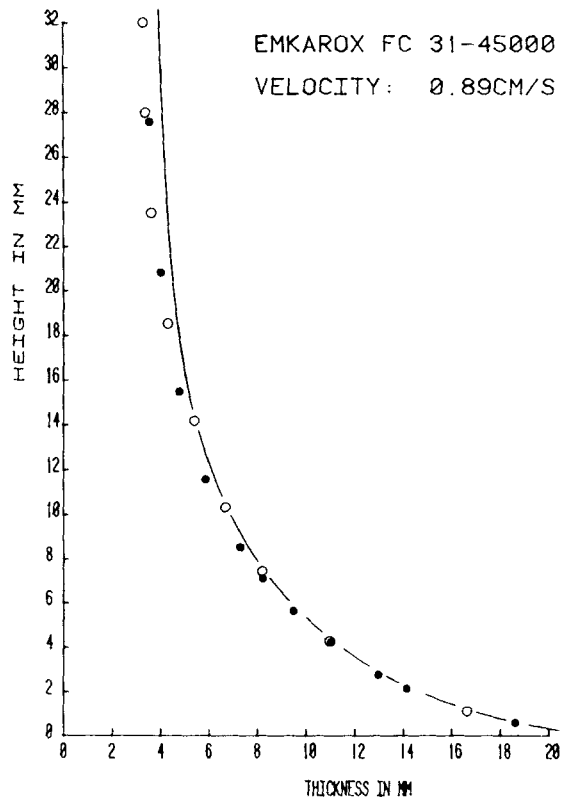

Figure 12. Meniscus profile for Emkarox FC 31-45000 ($V_0 = 0{\cdot}89$ cm/s): ○ numerical prediction; ● experimental measurement; — meniscus profile in the Newtonian case (same viscosity as that of Emkarox)

4.2.2. *Second-order fluid.* We have used the Emkarox 31-45000 which exhibits a Newtonian behaviour in viscosity and a second-order behaviour for the first normal stress difference. The parameters of equation (2) for this fluid have been taken from Reference 3, namely $\eta_0 = 124$ Pa.s and $\Psi_1 = 0{\cdot}04$ Pa.s^2. The particularity of this fluid is that it is the only one, to our knowledge, which can be called a real second-order fluid.

In Figure 12, as well as in Table III, the numerical predictions are compared with experimental data, showing very good agreement. In Figure 12, we also present the meniscus profile obtained when the Newtonian model (with the same value of viscosity) is introduced, in order to identify the influence of the second-order term of equation (2). The presence of the first normal stress difference (in other words, of some elasticity) tends to decrease the eventual coating thickness. Another very interesting point has to be outlined: the contribution of elongational flow appears to be correctly taken into account by the second-order model describing the rheological behaviour of the fluid used.

5. CONCLUSIONS

The augmented Lagrangian coupled to a finite element method is very suitable to simulate various non-Newtonian flows and in particular the dip coating process. The decoupling of non-linearities allows a great flexibility for introducing various complex rheological behaviours in the equations governing the dynamics of polymeric liquids.

We have shown that the role of elasticity is to reduce the eventual coating thickness.

Because the majority of the polymeric liquids exhibit both shear-thinning and elastic properties, the use of GNF models which take into account the former has not been found to adequately simulate the dip coating process.

We then underline the necessity of applying this method with more representative rheological behaviours.

ACKNOWLEDGEMENTS

The authors wish to acknowledge financial support provided by the NSERC of Canada.

REFERENCES

1. P. Tanguy, M. Fortin and L. Choplin, 'Finite element simulation of dip coating, I: Newtonian fluids', *Int. J. numer. methods fluids*, **4,** 441–457 (1984).
2. R. B. Bird, R. C. Armstrong and O. Hassager, in *Dynamics of polymeric Liquids, Vol. I: Fluid mechanics*, Wiley, New York, 1977.
3. L. Choplin, P. J. Carreau and A. Ait Kadi, 'Highly elastic-constant viscosity fluids', *Polym. Eng. Sci.*, **23,** 459 (1983).
4. M. A. Mendelson, P. W. Yeh, R. A. Brown and R. C. Armstrong, 'Approximation error in finite element calculation of viscoelastic fluid flows', *J. Non-Newt. Fluid Mech.*, **10,** 31 (1982).
5. M. Fortin and R. Glowinski, *Résolution Numérique de Problèmes aux Limites par des Méthodes de Lagrangien Augmenté*' Dunod, Paris, 1982.
6. A. Marrocco, 'Expériences numériques sur des problèmes non linéaires résolus par éléments finis et lagrangien augmenté' *Rapport Laboria No. 309*, INRIA, Rocquencourt, France, 1978.
7. M. Hestenes, 'Multiplier and gradient methods', *J. Optim. Theor. Appl.*, **4,** 303 (1969).
8. M. J. D. Powell, 'A method for non-linear constraints in minimization problems', in R. Fletcher (ed.) *Optimization*, Chap. 19, Academic Press, London, 1969.
9. P. J. Carreau, 'Rheological equations from molecular network theories', *Trans. Soc. Rheol.*, **16,** 99 (1972).
10. J. N. Lyness and D. Jespersen, 'Moderate degree symmetric quadratic rules for the triangle', *J. Inst. Math. Applic.*, **15,** 19 (1975).
11. P. J. Carreau, D. DeKee and M. Daroux, 'An analysis of the viscous behaviour of polymeric solutions', *Can. J. Chem. Eng.*, **57,** 135 (1979).
12. P. Tanguy, L. Choplin, M. Fortin and M. Robichaud, 'Dip Coating with second-order fluids', submitted to *J. Non-Newt. Fluid Mech.*